3D anisotropic wavefront-oriented ray tracing

Tina Kaschwich and Dirk Gajewski

email: *kaschwich@dkrz.de*
keywords: *ray tracing, traveltimes, anisotropic media*

ABSTRACT

Seismic traveltimes are required for a variety of applications. We present a wavefront-oriented ray-tracing technique for the computation of traveltimes in a smooth 3D anisotropic model. In this method, we propagate a wavefront stepwise through the model and interpolate output quantities (e.g., traveltime, slowness) from rays to gridpoints. In contrast to isotropic media, where the input is a velocity model, the model for an anisotropic medium is defined by 21 elastic parameters at each gridpoint. To interpolate the elastic parameters to arbitrary points we use the Cardinal spline interpolation. For a homogeneous transversely isotropic medium a comparison with reference traveltimes for qP-waves shows that the maximum absolute errors do not exceed 0.04 ms. In addition we compute traveltimes for an inhomogeneous triclinic model. While we have no analytical solutions to verify the computed traveltimes, we compared our results to traveltimes computed by an FD perturbation method.

INTRODUCTION

Seismic traveltimes are used in many processing techniques, such as Kirchhoff migration and traveltime tomography. There are two major approaches for the computation of traveltimes in anisotropic media: ray-tracing methods (see, e.g., Červený, 1972; Gajewski and Pšenčik, 1987) and methods which are based on a numerical solution of the eikonal equation using finite differences and perturbation (see, e.g., Ettrich and Gajewski, 1998; Lecomte, 1993). The main criteria to compare these methods are the accuracy and the efficiency (Leidenfrost et al., 1999).

Unfortunately, the traditional, i.e. two-point ray-tracing method is computationally expensive when traveltimes are required for an entire 2D or 3D grid. During the last years several authors have introduced new ray-tracing based methods, so called wavefront construction methods (Vinje et al., 1993; Lambaré et al., 1996). The basic idea of wavefront construction is to propagate a ray field rather than a single ray. For anisotropic media the propagation is performed by solving the kinematic ray-tracing system introduced by Červený (1972).

In the last year Coman and Gajewski (2001) presented an implementation to compute traveltimes by wavefront-oriented ray tracing in inhomogeneous isotropic media. Based on this efficient and accurate technique for isotropic media, we now extended the wavefront-oriented ray-tracing technique to compute qP-wave traveltimes in smooth 3D anisotropic media. Since we wish to consider arbitrary types of symmetry the 3D model for an anisotropic medium is defined by 21 elastic parameters and the density for every gridpoint. This leads to a more complicated formalism for the kinematic ray-tracing system than for isotropic media. Therefore we had to change the representation of the model: Instead of using trilinear interpolation, we compute the elastic parameters and the derivatives at arbitrary points by Cardinal spline interpolation. This makes the algorithm more efficient in terms of computational storage and CPU time.

After an introduction to the method we give several numerical examples. We demonstrate the accuracy of the method by comparing the traveltimes computed for a homogeneous transversely isotropic model to exact traveltimes. While we have no analytical solutions for an inhomogeneous anisotropic model, we compare our results with an alternative method for traveltime computation, the FD perturbation method

(Soukina and Gajewski, 2001).

THE METHOD

The wavefront-oriented ray-tracing technique presented by Coman and Gajewski (2002) for a smooth 3D isotropic medium is based on the idea of wavefront construction (WFC). Our implementation is an extension of this method to 3D smooth anisotropic media. In this part, we give a short overview of the theoretical background, i.e. the formalism of the kinematic ray-tracing system and the definition of the initial conditions in anisotropic media. Also, we explain some implementation details of the algorithm, e.g., the interpolation of the elastic parameters.

The kinematic ray-tracing system

The ray field is propagated by kinematic ray tracing (KRT). For the 3D anisotropic case the KRT-system is given by, e.g., Červený (2001),

$$\frac{\mathrm{d}x_i}{\mathrm{d}\tau} = a_{ijkl}p_l D_{jk}/D, \quad \frac{\mathrm{d}p_i}{\mathrm{d}\tau} = -\frac{1}{2}\frac{\partial a_{jkln}}{\partial x_i}p_k p_n D_{jl}/D. \tag{1}$$

The Einstein summation convention applies over all repeated lower indices and a_{ijkl} represents the density-normalised elastic tensor, x_i are the Cartesian coordinates; p_i are the components of the slowness vector $\vec{p}$, and τ is the traveltime along the ray. The D_{jk} and D are given by (see, e.g., Červený, 2001):

$$\begin{aligned}
D_{11} &= (\Gamma_{22} - G_m)(\Gamma_{33} - G_m) - \Gamma_{23}^2, \\
D_{22} &= (\Gamma_{11} - G_m)(\Gamma_{33} - G_m) - \Gamma_{13}^2, \\
D_{33} &= (\Gamma_{11} - G_m)(\Gamma_{22} - G_m) - \Gamma_{12}^2, \\
D_{12} = D_{21} &= \Gamma_{13}\Gamma_{23} - \Gamma_{12}(\Gamma_{33} - G_m), \\
D_{13} = D_{31} &= \Gamma_{12}\Gamma_{23} - \Gamma_{13}(\Gamma_{22} - G_m), \\
D_{23} = D_{32} &= \Gamma_{12}\Gamma_{13} - \Gamma_{23}(\Gamma_{11} - G_m), \\
D &= D_{11} + D_{22} + D_{33}.
\end{aligned} \tag{2}$$

The quantity G_m is the m-th eigenvalue of the Christoffel matrix Γ_{ik}, where m denotes the type of elementary wave we wish to compute (e.g., qP- or qS-wave). The Christoffel matrix is given by the relation

$$\Gamma_{ik} = a_{ijkl}p_j p_l. \tag{3}$$

Furthermore, the eikonal equation

$$G_m = \Gamma_{ik}D_{ik}/D = a_{ijkl}p_j p_l D_{ik}/D = 1 \ \text{ for } \ m = 1, 2, 3 \tag{4}$$

is satisfied along the ray. Therefore, Equation (4) should be taken into account in Equation (2).
The ray-tracing system (1) is identical for all types of waves (e.g., qP-wave or qS-wave) that can propagate in an anisotropic smooth inhomogeneous medium. Therefore, the type of wave is specified by the initial conditions, which are introduced in the next section.

Initial conditions

In contrast to the isotropic case the directions of the slowness vector $\vec{p}$ and the ray velocity vector $\vec{U}$ are different in an anisotropic medium. The direction of propagation of the wavefront is specified by the unit vector $\vec{N}$, given by the direction of the slowness vector $\vec{p} = \vec{N}/C$, and of the phase velocity C, where $C = [p_i p_i]^{-1/2}$.
The initial conditions for a single ray of one particular selected wave passing through a point S, the source position, can be most easily expressed by defining the initial direction of slowness vector $\vec{p}$ at the point S. The initial conditions for the ray tracing system (1) may then be expressed by

$$\text{at } S: \quad x_i^{(m)} = x_{i0}^{(m)}, \quad p_i^{(m)} = p_{i0}^{(m)}, \quad m = 1, 2, 3, \tag{5}$$

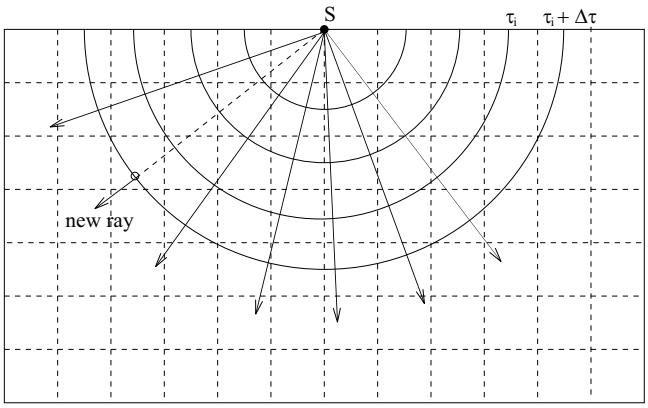

Figure 1: Graphical description of the WFC methods: the propagation of the ray field with a constant traveltime step $\Delta\tau$. If necessary, we insert a new ray by tracing it directly from the source

where $p_{i0}^{(m)}$ satisfy the eikonal equation (4) at the source location S corresponding to the particular wave denoted by m. To express the slowness $p_{i0}^{(m)}$, we define the components of the phase normal vector $\vec{N}_0$ using the take-off angles, i_0 and ϕ_0 at the source

$$N_{10} = \sin i_0 \cos \phi_0, \quad N_{20} = \sin i_0 \sin \phi_0, \quad N_{30} = \cos i_0. \tag{6}$$

After solving the eigenvalue problem to compute the phase velocity at the source $C_0^{(m)}$, the components of the slowness vector $\vec{p}^{(m)}$ at S are given by

$$p_{10}^{(m)} = N_{10}/C_0^{(m)}, \quad p_{20}^{(m)} = N_{20}/C_0^{(m)}, \quad p_{30}^{(m)} = N_{30}/C_0^{(m)}. \tag{7}$$

Propagation of wavefronts

The first step is the definition of a single ray by its initial conditions (5). To increase the efficiency the wavefront construction methods propagate a ray field rather than a single ray (see also Figure 1). To propagate the wavefront stepwise through the model we solve the KRT-system (1) for every timestep $\Delta\tau$ using a fourth-order Runge-Kutta method. To provide a high accuracy the ray density is evaluated after every timestep and, if necessary, new rays are inserted. The insertion of a new ray is performed by tracing it from the source (see Coman and Gajewski, 2001). To decide if a new ray has to be inserted three criteria are applied: (1) the distance between two adjacent rays exceeds a predefined threshold, (2) the difference in wavefront curvature between two adjacent rays exceeds a predefined threshold, (3) two adjacent rays cross each other. If one of the insertion criteria is satisfied, we insert a new ray by tracing it directly from the source. The initial conditions for the inserted ray are defined by halving of intervals of the initial conditions of the parent rays at the source S.

Using the KRT-system (1) we get the traveltime along the ray, but for Kirchhoff depth migration the traveltimes are needed on a rectangular grid. Therefore, we interpolate the output quantities on a Cartesian grid (for details see Coman and Gajewski, 2001). The wavefront curvature is needed for the interpolation to the grid. To make the method more efficient we use the position and the direction of the slowness for two adjacent rays and then approximate the wavefront curvature, instead of using dynamic ray tracing.

For Kirchhoff migration traveltimes on fine grids are needed. From the point of computational effiency it is advisable to calculate traveltimes on a coarse grid and then interpolate onto the fine grid, using, e.g., the hyperbolic interpolation by Vanelle and Gajewski (2002).

Following Vinje et al. (1996), we start with 12 rays from the source point which pass through the vertices of an icosahedron. To increase the ray density leaving from the source vicinity additional rays are introduced by interpolation on the surfaces of the icosahedron. Usually we start with 320 rays, which corresponds to two repeated interpolation steps.

Representation of the model

For our implementation we need the model defined on a discrete regular grid. In a complex inhomogeneous medium 21 elastic parameters and the density are required for each gridpoint. For the evaluation of the elastic parameters at arbitrary points, we used the Cardinal spline interpolation (Thomson and Gubbins, 1982).
To use the Cardinal spline interpolation instead of, for example, the cubic splines has significant advantages in terms of computational storage and time. If we used cubic splines (Späth, 1973) we would have to calculate four coeffients for each grid increment in each dimension. For a model defined on a $101 \times 101 \times 101$ grid cube, we would thus have to compute and store $64.000.000$ coefficients. Using the Cardinal spline interpolation we have to calculate and store only about 400 values (depends on the chosen accuracy of the interpolation). The elastic parameters at an arbitrary point are interpolated from the nearest gridpoint where the parameters are known, using the distance between the points as weighting term.
Also, using Cardinal splines instead of, e.g., linear interpolation, we can compute the first spatial derivatives of the elastic parameters, which are needed to solve the KRT-system, without storing them on the regular grid.

NUMERICAL RESULTS

To illustrate the accuracy of the traveltime computation by wavefront-oriented ray tracing in 3D anisotropic media we chose two types of models. To estimate the accuracy we considered a homogeneous transversely isotropic model, because here we know the exact solutions. We use the Voigt-notation A_{mn} for the density-normalised tensor a_{ijkl} with the usual correspondence $m \rightarrow i,j$ and $n \rightarrow k,l$: $1 \rightarrow 1,1$; $2 \rightarrow 2,2$; $3 \rightarrow 3,3$; $4 \rightarrow 2,3$; $5 \rightarrow 1,3$; $6 \rightarrow 1,2$. The density-normalised elastic parameters of the example medium are given by

$$\underline{A} = \begin{pmatrix} 15.96 & 6.99 & 6.06 & 0.00 & 0.00 & 0.00 \\ & 15.96 & 6.06 & 0.00 & 0.00 & 0.00 \\ & & 11.40 & 0.00 & 0.00 & 0.00 \\ & & & 2.22 & 0.00 & 0.00 \\ & & & & 2.22 & 0.00 \\ & & & & & 4.48 \end{pmatrix} [km^2/s^2]. \tag{8}$$

A model cube of $100 \times 100 \times 100$ is considered. The grid spacing is 10 m in each direction. The source point is located in the center of the x-y plane and in a depth of 60m at the position $(0.5, 0.5, 0.06$km$)$. The results of the comparison between exact traveltimes and traveltimes computed by wavefront-oriented ray tracing are shown in Figure 2. Usually, we have the highest wavefront curvature near the source. Therefore, the maximum relative error of 0.11% is located in this region. The relative errors near the source appear exaggerated since there the traveltimes themselves are very small. The observed average relative error is only $1.15 \cdot 10^{-3}\%$. In addition, we show the absolute traveltime error (see Figure 3(a)). The maximal absolute error $4 \cdot 10^{-2}$ms is located in the source region. We observed an average absolute error of $1 \cdot 10^{-3}$ms. Figure 2(b) visualises that we have for the most part of the model only random numerical errors. For this homogeneous anisotropic model the traveltimes computed with our implementation are nearly exact.

Since we have no exact traveltimes for a heterogeneous anisotropic medium, we compare traveltimes calculated by wavefront-oriented ray tracing with traveltimes obtained by the FD perturbation method (Soukina and Gajewski, 2001). To estimate the error distribution for both methods, we calculate the absolute traveltime error for the homogeneous anisotropic model and use this knowledge for a heterogeneous anisotropic model.
In Figure 3 the absolute traveltime errors in comparison to the FD perturbation method (Soukina and Gajewski, 2001) are shown. The FD perturbation method accumulates absolute traveltime errors with increasing distance from the source location (see Figure 3(b)). The wavefront-oriented ray tracing has only small errors in the source region, and the absolute error distribution in the rest of the model is nearly homogeneous. We use this knowledge about the error distribution for both methods to assess the quality of our implementation for traveltimes in a heterogeneous anisotropic model.

As an inhomogeneous anisotropic example we used a factorised anisotropic medium (FAM). FAM were

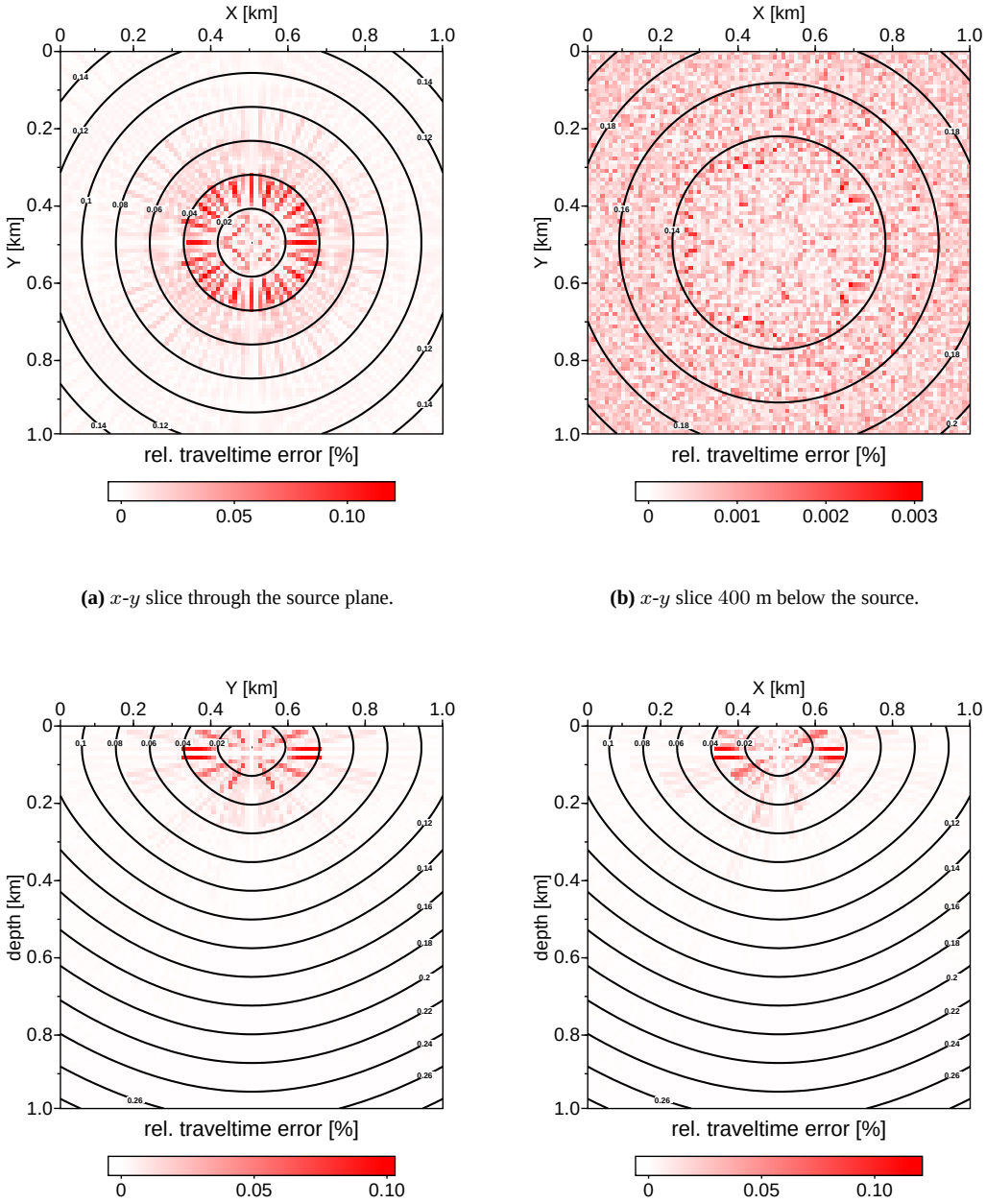

(a) x-y slice through the source plane.

(b) x-y slice 400 m below the source.

(c) y-z slice through the source

(d) x-z slice through the source

Figure 2: Wavefronts in a homogeneous transversely isotropic model. The upper figures shows slices with different distances in depth from the source location $(0.5, 0.5, 0.06$ km). The figures below shows vertical slices through the source position. The underlying greyscale images show the relative errors. Please note the different error scales.

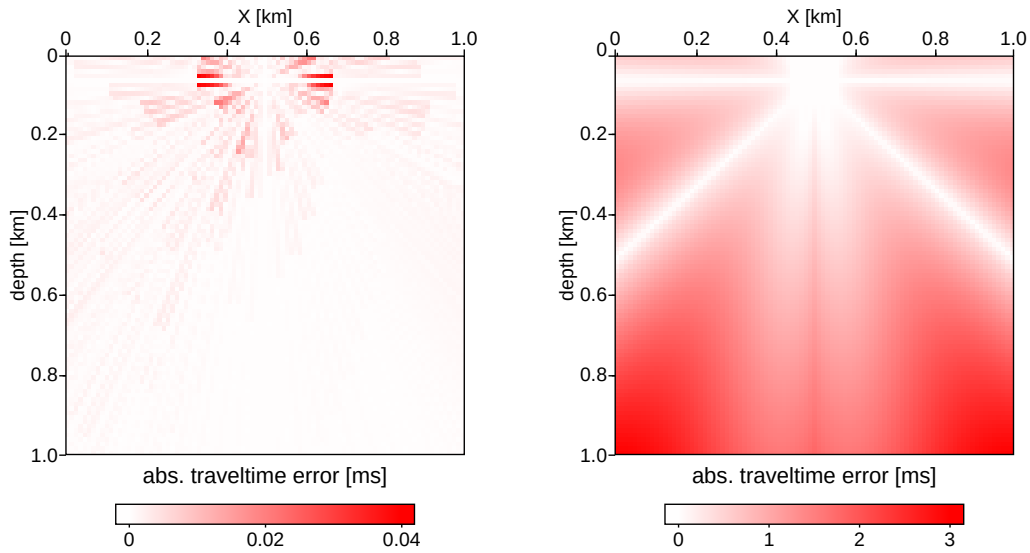

(a) Wavefront-oriented ray tracing

(b) FD perturbation method

Figure 3: Absolute traveltime errors for the homogeneous transversely isotropic model, both figures shows a x–z slice to represent the error distribution for the different methods; left: wavefront-oriented ray tracing; right: FD perturbation method. Please note the different error scales.

introduced by Červený (1989). To construct FAM we multiplied the same elastic parameters by an individual factor for each gridpoint.
The elastic parameters for the triclinic sandstone are (Mensch and Rasolofosaon, 1997):

$$\underline{A} = \begin{pmatrix} 6.77 & 0.62 & 1.0 & -0.48 & 0.00 & -0.24 \\ & 4.95 & 0.43 & 0.38 & 0.67 & 0.52 \\ & & 5.09 & -0.28 & 0.09 & -0.09 \\ & & & 2.35 & 0.09 & 0.00 \\ & & & & 2.45 & 0.00 \\ & & & & & 2.88 \end{pmatrix} [km^2/s^2]. \tag{9}$$

For the uppermost 100m the factor has the constant value 3.0, underneath the factor increased linearly with depth up to a value of 3.4 at the bottom of the model. The size of the model and the location of the source are as in the first example. Figure (4) shows the calculated differences between traveltimes from the FD perturbation method and the traveltimes obtained by wavefront-oriented ray tracing. The solid lines display the wavefronts calculated by our method, whereas the dotted lines visualise the results from the FD perturbation method. The maximum absolut traveltime difference is 2.3 ms and we observed an average absolute traveltime difference of 0.6 ms. It can be seen, that the behaviour and the order of traveltime differences are similar to the observed errors in the previous model.
In conclusions of these observations, the accuracy of the anisotropic wavefront-oriented ray tracing is nearly constant over the whole 3D model. Although the FD perturbation method is faster, its accuracy decreases with growing distance from the source.

CONCLUSIONS

We have presented a new implementation to compute traveltimes in 3D heterogeneous anisotropic media with arbitrary symmetry based on wavefront-oriented ray tracing. We have shown the representation of the model, which is defined by the elastic parameters. The elastic parameters on arbitrary positions are

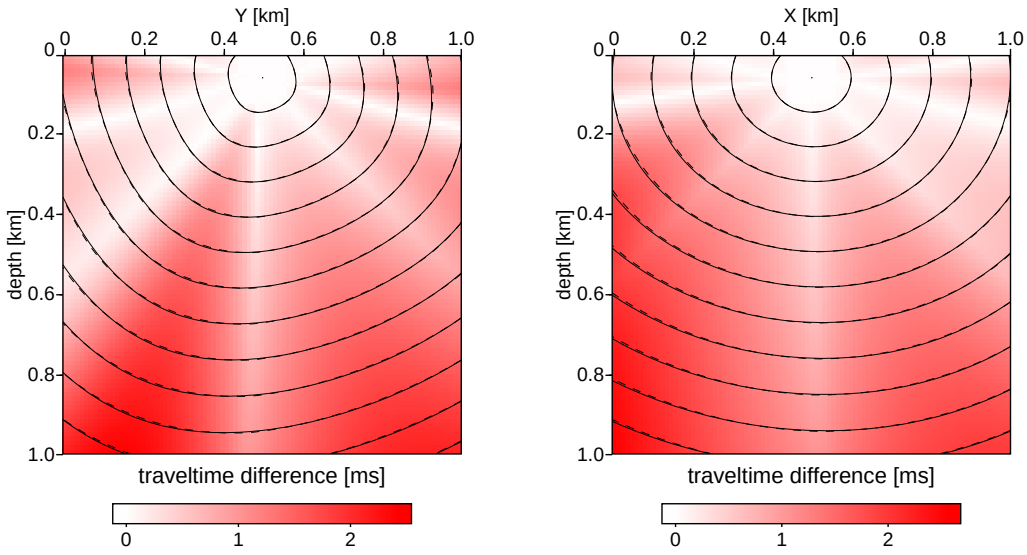

(a) y-z slice through the source plane

(b) x-z slice 400m below the source

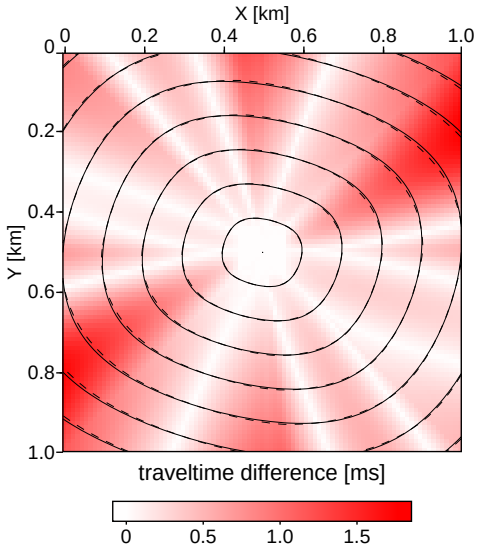

(c) x-y slice through the source

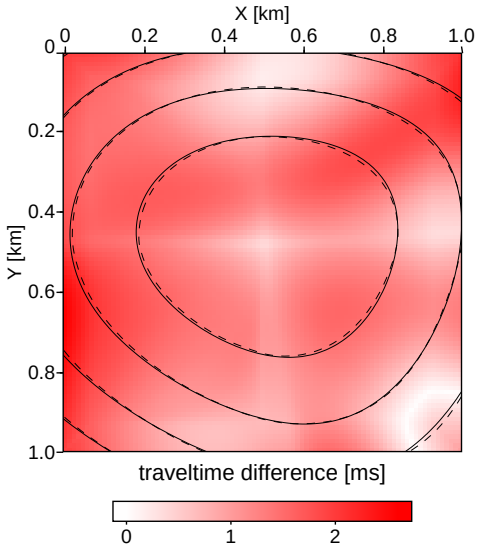

(d) x-y slice through the source

Figure 4: Wavefronts for the factorised triclinic anisotropic model. The solid lines show the wavefronts calculated by wavefront-oriented ray tracing, whereas the dotted lines represent the traveltimes obtained by the FD perturbation method. The underlying greyscale illustrates the absolute traveltime error between both methods in ms.

computed by Cardinal spline interpolation. A first numerical example illustrates the accuracy of our method for the computation of traveltimes of qP-waves in a homogeneous transversely isotropic model. We have also evaluated the computation of traveltimes in a heterogeneous anisotropic model. There we compared the traveltimes calculated by wavefront-oriented ray tracing to traveltimes obtained by a FD perturbation method.
In general, the method is valid for qS-waves also, if we assume that we have two well-separated qS waves. That means we have strongly anisotropic media and no shear wave singularities. Therefore, future work must be devoted to calculate numerical examples for qS-waves in inhomogeneous anisotropic models.

ACKNOWLEDGEMENTS

This work was supported by the *German Research Society (DFG, Ga 350-10)* and the sponsors of the *Wave Inversion Technology (WIT) Consortium*. Continuous discussions with the members of the Applied Geophysics Group Hamburg including Boris Kashtan are appreciated. We thank Radu Coman for providing his source code.

REFERENCES

Červený, V. (1972). Seismic Rays and Ray Intensities in Inhomogeneous Anisotropic Media. *The Geophysical Journal of the Royal Astronomical Society*, 29:1–13.

Červený, V. (1989). Ray tracing in factorized anisotropic inhomogeneous media . *Geophysical Journal International*, 99:91–100.

Červený, V. (2001). *Seismic Ray Theory*. Cambridge University Press.

Coman, R. and Gajewski, D. (2001). Traveltime computation by wavefront-oriented ray tracing. *Annual report No.6, WIT Consortium*, pages 231–244.

Coman, R. and Gajewski, D. (2002). 3-D wavefront-oriented ray tracing: Estimation of traveltimes within cells. *Annual report No.6, WIT Consortium*.

Ettrich, N. and Gajewski, D. (1998). Traveltime computation by perturbation with FD-eikonal solvers in isotropic and weakly anisotropic media. *Geophysics*, 63:1066–1078.

Gajewski, D. and Pšenčik, I. (1987). Computation of high-frequency seismic wavefields in 3-D laterally inhomogeneous anisotropic media. *The Geophysical Journal of the Royal Astronomical Society*, 91:383–411.

Lambaré, G., Lucio, P., and Hanyga, A. (1996). Two-dimensional multivalued traveltime and amplitude maps by uniform sampling of a ray field. *Geophysical Journal International*, 125:584–598.

Lecomte, I. (1993). Finite difference calculation of first traveltimes in anisotropic media. *Geophysical Journal International*, 113:318–342.

Leidenfrost, A., Ettrich, N., Gajewski, D., and Kosloff, D. (1999). Comparison of six different methods for calculating traveltimes. *Geophysical Prospecting*, 47:269–297.

Mensch, T. and Rasolofosaon, P. (1997). Elastic-wave velocities in anisotropic media of arbitrary symmetry- generalization of Thomsen's parameters ϵ, δ, γ . *Geophysical Journal International*, 128:1070–1088.

Soukina, S. and Gajewski, D. (2001). A traveltime computation in 3-D anisotropic media by a finite-difference pertubation method. *Annual report No.5, WIT Consortium*, pages 254–267.

Späth (1973). *Spline-Algoritmen zur Konstruktion glatter Kurven und Flächen*. R. Oldenbourg Verlag München Wien.

Thomson, C. and Gubbins, D. (1982). Three-dimensional lithospheric modelling at NORSAR: linearity of the method and amplitude variations from the anomalies. *The Geophysical Journal of the Royal Astronomical Society*, 71:1–36.

Vanelle, C. and Gajewski, D. (2002). Second-order interpolation of traveltimes. *Geophysical Prospecting*, 50:73–83.

Vinje, V., Iversen, E., Åstebøl, K., and Gjøystdal, H. (1996). Estimation of multivalued arrivals in 3D models using wavefront construction- Part I. *Geophysical Prospecting*, 44:819–842.

Vinje, V., Iversen, E., and Gjøystdal, H. (1993). Traveltime and amplitude estimation using wavefront construction. *Geophysics*, 58:8:1157–1166.